# Thesis Title

## Thomas P. Ogden

---

**Abstract**

Here is my abstract.

# Thesis Title

## Thomas P. Ogden

A thesis submitted in partial fulfilment
of the requirements for the degree of
Doctor of Philosophy.



Department of Physics

Durham University

December 20, 2015

# *Declaration*

I confirm that no part of the material offered has previously been submitted by myself for a degree in this or any other University. Where material has been generated through joint work, the work of others has been indicated.

Thomas P. Ogden

Durham, December 20, 2015

*Dedicated to Someone Special,*

*for some special reason.*

# Contents

# 1 Introduction

# 2 Propagation of Light in Thermal Atomic Vapours

## 2.1 Introduction

In this chapter we will define the model for propagation in thermal atoms to be used throughout the thesis, based on the well-known Maxwell Bloch (MB) equations. We will introduce the concept of susceptibilities and discuss analytic solutions to the equations that are available in the regime of weak incident light, before generalising the problem to nonlinear interaction with quantised atoms. Finally we will present results from numerical solutions and compare with the analytic results for weak fields to verify the accuracy of the numerical model.

## 2.2 Deriving the Propagation Equation

In this section we will derive an equation to describe the propagation of a classical elecromagnetic field in a polarised medium. Our starting point, naturally, is Maxwell's set of equations of classical electrodynamics.

9

## 2.2.1 Maxwell's Equations and the Wave Equation

In a medium with no free charges or free current, Maxwell's equations for the electric field $\mathbf{E}$ and the magnetic field $\mathbf{B}$ can be written[1]

$$\nabla \cdot \mathbf{D} = 0 \tag{2.1a}$$

$$\nabla \cdot \mathbf{B} = 0 \tag{2.1b}$$

$$\nabla \times \mathbf{E} = -\frac{\partial \mathbf{B}}{\partial t} \tag{2.1c}$$

$$\nabla \times \mathbf{B} = \mu_0 \frac{\partial \mathbf{D}}{\partial t}. \tag{2.1d}$$

The electric displacement $\mathbf{D}$ accounts for the effect of charges in a medium and is given by

$$\mathbf{D} = \varepsilon_0 \mathbf{E} + \mathbf{P} \tag{2.2}$$

where $\varepsilon_0$ is the vacuum permittivity and the electric polarisation $\mathbf{P}$ describes the cumulative effect of induced dipole moments in individual atoms. We'll discuss the source of polarisation in atoms further in section 2.3.

Taking the curl of (2.1c) and substituting (2.1d) we find

$$\nabla \times (\nabla \times \mathbf{E}) = -\mu_0 \frac{\partial \mathbf{D}^2}{\partial t^2}.$$

We then apply the vector identity

$$\nabla \times (\nabla \times \mathbf{E}) = \nabla(\nabla \cdot \mathbf{E}) - \nabla^2 \mathbf{E}$$

and, assuming that the polarisation varies little in the plane transverse to propagation such that $\nabla \cdot \mathbf{P} \approx 0$, arrive at the Maxwell wave equation

$$\nabla^2 \mathbf{E} - \frac{1}{c^2} \frac{\partial^2 \mathbf{E}}{\partial t^2} = \mu_0 \frac{\partial^2 \mathbf{P}}{\partial t^2}. \tag{2.3}$$

The Maxwell wave equation (MWE) thus describes the wave-like propagation of an electric field $\mathbf{E}$ through a medium with polarisation $\mathbf{P}$. The

second derivative on the right-hand side tells us that the accelerating charges described by **P** can act as a source of new components of the electromagnetic field. For this reason, polarisation plays a critical role in practically all optical phenomena.[2]

A similar propagation equation to (2.3) may be derived for the magnetic field, however we'll find that the interaction of atoms with the electric field dominates and so we will not consider **B** further.

We will consider 1D propagation along the z-axis, a restriction well-justified by the deconstructive interference of light scattered by atomic dipoles in directions not aligned with the incident radiation.[3] Then we might write the transverse field as $\mathbf{E} = \hat{\mathbf{x}}E(z,t)$, where $\hat{\mathbf{x}}$ is a unit vector perpendicular to $z$. We assume that we are dealing with atoms that are electrically neutral to start with, such that all of the polarisation in the medium will be induced by that field, so we may similarly set $\mathbf{P} = \hat{\mathbf{x}}P(z,t)$. In this way we can reduce the MWE to the scalar form

$$\frac{\partial^2 E}{\partial z^2} - \frac{1}{c^2}\frac{\partial^2 E}{\partial t^2} = \mu_0 \frac{\partial^2 P}{\partial t^2}. \tag{2.4}$$

In the absence of sources (i.e. $P = 0$) we can solve the homogeneous equation (2.4) analytically. For a nonconducting medium with spatially constant permeability and susceptibility the solution is a transverse monochromatic plane wave[1]

$$\tilde{E}(z,t) = \tilde{E}_0 e^{i(kz - \omega t)}. \tag{2.5}$$

where as usual $k$ represents wavenumber and $\omega$ the angular frequency. The amplitude is given by $\tilde{E}_0$. Of course, the electric field is an observable physical quantity and so must be real-valued — it is the real part of the complex $\tilde{E}(z,t)$ given by

$$E(z,t) = \Re[\tilde{E}(z,t)] = \tfrac{1}{2}\tilde{E}_0(z,t)e^{i(kz-\omega t)} + \tfrac{1}{2}\tilde{E}_0^*(z,t)e^{-i(kz-\omega t)}. \tag{2.6}$$

We continue with the complex notation for the usual reason that manipulations, such as adding components of different phases, are much simpler.

By substituting (2.5) into (2.4) we obtain the simplest *dispersion relation* of $\omega = ck$, *i.e.* all frequencies travel at a speed $c$, a familiar result for light in vacuo. Such plane wave solutions will propagate without attenuation or dispersion, which is how we are able to look up at the night sky and observe light from distant stars that has travelled enormous distance through the void of interstellar space.

Light travelling through matter is a more complex problem. We next want to look for solutions to (2.4) in the presence of sources, such that we have $P \neq 0$ describing induced atomic dipoles in the medium. For that we will need to make a useful approximation.

### 2.2.2 *The Slowly Varying Envelope Approximation*

If the spectrum of the electric field is narrowband, we approximate the field as the product of a quasi-monochromatic *carrier* function with angular frequency $\omega$ and wavenumber $k$ and a *slowly-varying envelope*

$$E(z,t) = \tfrac{1}{2}\mathcal{E}(z,t)e^{i(kz-\omega t)} + \tfrac{1}{2}\mathcal{E}^*(z,t)e^{-i(kz-\omega t)} \tag{2.7}$$

where the envelope is in general a complex function

$$\mathcal{E}(z,t) = |\mathcal{E}|e^{i\varphi}. \tag{2.8}$$

We apply the same treatment to the polarisation

$$P(z,t) = \tfrac{1}{2}\mathcal{P}(z,t)e^{i(kz-\omega t)} + \tfrac{1}{2}\mathcal{P}^*(z,t)e^{-i(kz-\omega t)} \tag{2.9}$$

with a polarisation envelope

$$\mathcal{P}(z,t) = |\mathcal{P}|e^{i\varphi}. \tag{2.10}$$

We can substitute these into (2.4) and by matching co-rotating terms we find

$$\left[ (\partial_{zz} + 2ik\partial_z - k^2) - \frac{1}{c^2}(\partial_{tt} - 2i\omega\partial_t - \omega^2) \right] \mathcal{E} = \mu_0 (\partial_{tt} - 2i\omega\partial_t - \omega^2)\mathcal{P}.$$

(2.11)

Now we're set to make the *slowly-varying envelope approximation*.[4] If the envelope changes only a small amount over the distance of a wavelength, and over the duration of the optical period, we can take

$$|\partial_{zz}\mathcal{E}| \ll k|\partial_z\mathcal{E}|$$

$$|\partial_{tt}\mathcal{E}| \ll \omega|\partial_t\mathcal{E}|$$

and neglect the second derivatives. Similar approximations hold for $\mathcal{P}$, where we may also neglect the first-order time derivative

$$|\partial_{zz}\mathcal{P}| \ll k|\partial_z\mathcal{P}|$$

$$|\partial_{tt}\mathcal{E}| \ll \omega|\partial_t\mathcal{E}|$$

$$|\partial_t\mathcal{P}| \ll \omega|\mathcal{P}|.$$

In the case of visible light with wavelengths on the order of 100 nm and optical periods of the order of 1 fs, where we're interested in the behaviour over ns or $\mu$s, this approximation is justified.

With these approximations made, (2.11) becomes

$$\left[ 2ik\partial_z - k^2 + \frac{1}{c^2}(2i\omega\partial_t + \omega^2) \right] \mathcal{E} = -\mu_0\omega^2\mathcal{P}$$

(2.12)

As the carrier wavenumber and frequency are still related by the vacuum dispersion relation $\omega = ck$ we then obtain the first-order propagation equation

$$\left[ \frac{\partial}{\partial z} + \frac{1}{c}\frac{\partial}{\partial t} \right] \mathcal{E} = i\frac{k}{2\epsilon_0}\mathcal{P}.$$

(2.13)

The wave equation (2.13), first-order in space $z$ and time $t$, can be solved numerically for a given medium, to determine how light will propagate through it. But we will next need to determine how the media through $\mathcal{P}$ is itself affected by the field $\mathcal{E}$.

### 2.2.3 Energy and Intensity

In an experiment we will not be measuring the electric field directly, but the energy transferred to a detector such as a photon counter. Also, any macroscopic measurement of light is necessarily going to extend over many optical cycles (of duration $\sim 10^{-15}$ s). So a property useful to us is the time-averaged power per unit area that the electromagnetic field transports through the medium, which we call the intensity $I$ and is calculated to be[5]

$$I = \tfrac{1}{2} c \varepsilon_0 |\mathcal{E}^2|. \tag{2.14}$$

## 2.3 Linear Optics, Susceptibility and Refractive Index

The effect of an electric field **E** applied on a single neutral atom is to separate the positively charged core (which moves in the direction of the field **E**) and the negatively charged electron cloud (which moves in the opposite direction $-$**E**) such that a dipole is induced on the atom parallel to the field. For an atomic vapour subject to a field, dipoles will be induced on many atoms. The cumulative effect is that the medium is polarised, and we define **P** as the dipole moment per unit volume.

### 2.3.1 Susceptibility

In general, the instantaneous polarisation induced by the field at a time $t$ is some function of the input field, which we may write as a power expansion[2] in **E**,

$$\mathbf{P}_{\text{inst}}(t) = \varepsilon_0 \left[ \chi^{(1)}(t)\mathbf{E}(t) + \chi^{(2)}(t)\mathbf{E}(t)^2 + \chi^{(3)}(t)\mathbf{E}(t)^3 + \dots \right] \tag{2.15}$$

where the expansion coefficients $\chi^{(j)}(t)$ are known as the $j$th- order susceptibilities.

If the applied field is weak, we find that the induced polarisation is proportional to that field, such that susceptibilities higher than $\chi^{(1)}$ are taken as zero and terms higher than the first order in (2.15) are neglected. This is the regime of *linear optics*. In this thesis we are particularly interested in developing and understanding numerical solutions of *nonlinear* problems, *i.e.* those in which higher order terms become significant. Systems involving weak fields are commonplace however, and as they permit analytic solution, along with offering insight into a broad range of optical phenomena, we will look at the linear regime briefly.

The cumulative induced polarisation $P(t)$ is an integral of the instantaneous polarisation over all times $t'$ previous

$$P(t) = \varepsilon_0 \int_{-\infty}^{t} \chi(t')E(t-t')\mathrm{d}t' \tag{2.16}$$

where we no longer require a superscript to define the linear susceptibility $\chi(t) := \chi^{(1)}(t)$. The upper limit on the integral expresses the causality condition that only the applied field at times in the past may affect the current state of the atoms.

So far we have described atomic response in the time domain, which is particularly useful when looking at time-dependent input fields such as short pulses. But it is also instructive to look at the frequency domain, which is advantageous when the input field is monochromatic. The change in perspective is effected as usual via the Fourier transform.[3] We will use the convention for the transform on the electric field envelope $\mathcal{E}(t)$

$$\mathcal{E}(\omega) = \int_{-\infty}^{\infty} \mathcal{E}(t)\mathrm{e}^{\mathrm{i}\omega t}\mathrm{d}t \tag{2.17}$$

and for the inverse

$$\mathcal{E}(t) = \frac{1}{2\pi} \int_{-\infty}^{\infty} \mathcal{E}(\omega)\mathrm{e}^{-\mathrm{i}\omega t}\mathrm{d}\omega \tag{2.18}$$

and we define the transform in the same way for the polarisation envelope $\mathcal{P}(t)$.

Making the envelope and carrier ansatz as in (2.33) and substituting (2.18) into the right-hand side of (2.16), we get

$$\mathcal{P}(t) = \varepsilon_0 \int_{-\infty}^{t} \chi(t') \frac{1}{2\pi} \int_{-\infty}^{\infty} \mathcal{E}(\omega) e^{-i\omega(t-t')} d\omega dt'. \tag{2.19}$$

We now define the frequency-dependent linear susceptibility

$$\chi(\omega) := \int_{-\infty}^{t} \chi(t') e^{i\omega t'} dt' \tag{2.20}$$

such that

$$\mathcal{P}(t) = \frac{1}{2\pi} \int_{-\infty}^{\infty} \varepsilon_0 \chi(\omega) \mathcal{E}(\omega) e^{-i\omega t} d\omega. \tag{2.21}$$

This expression gives the time-dependent polarisation in terms of the frequency components of the field weighted by that frequency-dependent susceptibility function. We may then take the Fourier transform of the left-hand side and, as the equality holds for each frequency, we obtain the frequency domain linear response function

$$\mathcal{P}(\omega) = \varepsilon_0 \chi(\omega) \mathcal{E}(\omega). \tag{2.22}$$

We may now substitute this expression into (2.13), with $\mathcal{E}(\omega)$ time-independent by the definition (2.17), to obtain

$$\frac{\partial \mathcal{E}(z,\omega)}{\partial z} = i\frac{k}{2}\chi(\omega)\mathcal{E}(z,\omega). \tag{2.23}$$

This first-order differential equation in $z$ has the analytical solution

$$\mathcal{E}(z,\omega) = e^{i\frac{k}{2}\chi z}. \tag{2.24}$$

Having determined an expression for the electric field envelope in terms of the frequency-dependent susceptibility, we can put this expression for the envelope into 2.13 in order to determine the effect it will have. It is useful to separate the real and imaginary parts of the susceptibility $\chi(\omega) := \chi_R(\omega) + i\chi_I(\omega)$, and we find

$$\mathcal{E}(z,\omega) = \mathcal{E}(0,\omega) e^{i(\frac{k}{2}\chi_R z)} e^{-\frac{k}{2}\chi_I z}. \tag{2.25}$$

The real part of the frequency dependent susceptibility then corresponds to a phase shift $\frac{k}{2}\chi_R z$ and so dispersion, and the imaginary part diminishes the field. As defined in (2.14) the intensity $I \propto |\mathcal{E}|^2$ and so is attenuated as it progresses through the medium via

$$I(z,\omega) = I_0(z,\omega)e^{-\alpha(\omega)z} \tag{2.26}$$

where the absorption coefficient $\alpha(\omega) := k\chi_I(\omega)$. This is the familiar Beer law of absorption for weak fields.

### 2.3.2 Refractive Index

If we return back to the Maxwell equations, we see by substitution of the susceptibility $\chi$ into the definition for dispersion (2.2), we get

$$\mathbf{D} = \varepsilon_0(1+\chi)\mathbf{E}. \tag{2.27}$$

Deriving the Maxwell wave equation again using this substitution, we find that the result is as for propagation in free space but with the vacuum speed $c$ replaced with a general phase velocity

$$v_p = \frac{c}{\sqrt{1+\chi}} = \frac{c}{n} \tag{2.28}$$

where $n$ is the refractive index, familiar from geometrical optics. In most linear media $\chi$ is positive, so light travels more slowly in the medium.[6]

This leads us to consider what this velocity represents, considering that photons are massless and must travel at $c$.[7] The resultant field wave is a superposition of the applied field wave and a secondary field wave which results from induced dipoles. In linear media, this resultant wave has the same carrier frequency but a different phase. The fact that the frequency is the same is the reason dense transparent materials exist. If the secondary wave lags the applied wave, the resultant wave will also lag. An observer in the medium will have to wait longer for the peaks

of the resultant wave to come past. It is this phase difference which leads to an apparently slower phase velocity. The refractive index represents the cumulative phase difference as the light moves through the medium.[3]

## 2.4   *Interaction of Light with Atoms*

We have seen in the weak field regime how the linear susceptibility relates to the absorptive and dispersive response of the medium. But we have not yet determined how that susceptibility relates to the properties of the atomic ensemble. Beyond the linear regime, the susceptibility is not a good descriptor for the response of the medium, and analytic expressions for the field propagation are not available. In the nonlinear regime, we will need to follow the dynamics of the atoms to determine how the field will propagate through the medium.

For the dynamics of atom-light interaction to be properly considered the system must be treated as an open quantum system. While the processes of absorption and stimulated emission (of photons from and to the applied field) can be described within a closed quantum system, the process of spontaneous decay due to interaction with vacuum fluctuations surrounding an atom cannot. As such, the time evolution is described by the Lindblad master equation

$$i\hbar \frac{\partial \rho}{\partial t} = [\mathcal{H}, \rho] + \mathcal{L}\{\rho\}. \tag{2.29}$$

The background of this equation and the conditions under which it is valid are discussed in appendix A. It constitutes a set of differential equations to be solved: one for each of the density matrix elements.

### 2.4.1   Spontaneous Decay of Excited States

As described in equation (A.9), coupling to the environment is imple-
mented via the Lindblad superoperator $\mathcal{L}$ which is completely defined
by a finite set of collapse operators. In the case of spontaneous emission
due to interaction with vacuum fluctuations, these are defined as

$$C_{ij} = \sqrt{\Gamma_{ij}} \, |i\rangle \, \langle j| . \tag{2.30}$$

where $\Gamma_{ij} = 1/\tau_{ij}$ and $\tau_{ij}$ is the stochastic rate at which electrons spon-
taneously decay from a higher state $|j\rangle$ to a lower state $|i\rangle$. The quantity
$\Gamma_{ij}$ is known as the natural linewidth for the specific transition $|i\rangle \rightarrow |j\rangle$,
for reasons that will be clarified in section 2.5.

### 2.4.2   The Interaction Hamiltonian

A single-electron (or hydrogenic) atom has a positively charged nucleus
and a negatively charged electron, both of which will interact with an
applied electromagnetic field. At optical wavelengths, however, the in-
teraction with the nucleus is negligible,[8] so we focus our attention on
the electron.

Without interaction with an external field, the bare atomic Hamiltonian
is given by

$$\mathcal{H}_0 = \frac{\mathbf{p}^2}{2m_e} + V(r) \tag{2.31}$$

where $m_e$ is the mass of the electron, $\mathbf{r}$ and $\mathbf{p} = i\hbar\nabla$ are its position and
momentum operators, and $V(r)$ is the spherical atomic potential.

The non-relativistic Hamiltonian of the electron interacting with an ap-
plied classical electric field $\mathbf{E}$, in the Coulomb gauge, may be written

$$\mathcal{H} = \mathcal{H}_0 + \mathcal{H}_I \tag{2.32}$$

where the interaction Hamiltonian term $\mathcal{H}_I$ describes the coupling of the atomic dipole to the field.[8] The problem of the atom-light interaction is then one of calculating the matrix elements of $\mathcal{H}_I$ as a perturbation to the eigenstate basis of $\mathcal{H}_0$.

We will consider a monochromatic field with angular frequency $\omega$ and wavenumber $\mathbf{k}$ (the analysis extends to multi-chromatic fields, which we will consider in chapter 3). We may write the field as

$$\mathbf{E}(\mathbf{r},t) = \hat{\mathbf{x}} \left[ \tfrac{1}{2}\mathcal{E}(t)e^{i(\mathbf{k}\cdot\mathbf{r}-\omega t)} + \tfrac{1}{2}\mathcal{E}^*(t)e^{-i(\mathbf{k}\cdot\mathbf{r}-\omega t)} \right] \tag{2.33}$$

where $\hat{\mathbf{x}}$ is the unit polarisation vector and $\mathcal{E}(t)$ is the field amplitude.

We simplify calculation of matrix elements by making the exponential expansion

$$e^{i\mathbf{k}\cdot\mathbf{r}} \approx 1 + (i\mathbf{k}\cdot\mathbf{r}) + \frac{1}{2!}(i\mathbf{k}\cdot\mathbf{r})^2 + \ldots \tag{2.34}$$

and neglecting all but the first term, unity. This *electric dipole approximation*[9] represents neglecting the spatial dependence of the field over the extent of the atom, and is justified as the electronic wavefunction is on the order of the Bohr radius at $10^{-10}$ m and the optical carrier wavelength $\lambda = 2\pi/k$ is on the order of $10^{-7}$ m. The approximation may equivalently be derived as truncating a multipole expansion of the interaction at the dipole term.[10]

Applying the electric dipole approximation, we may write the interaction Hamiltonian term as

$$\mathcal{H}_I = -e\mathbf{r}\cdot\mathbf{E} = -\mathbf{d}\cdot\mathbf{E} \tag{2.35}$$

where analogous with a classical dipole moment, $\mathbf{d}$ is the electric dipole operator. And we may take the field out of the spatial integral implicit in calculating the matrix elements between two bare atom eigenstates $|a\rangle$

and $|b\rangle$,

$$
\begin{aligned}
\langle a| \mathcal{H}_I |b\rangle &= - \left[ \tfrac{1}{2}\mathcal{E}(t)\mathrm{e}^{-\mathrm{i}\omega t} + \tfrac{1}{2}\mathcal{E}^*(t)\mathrm{e}^{\mathrm{i}\omega t} \right] \langle a| \hat{\mathbf{x}} \cdot e\mathbf{r} |b\rangle \\
&= - \left[ \tfrac{1}{2}\mathcal{E}(t)\mathrm{e}^{-\mathrm{i}\omega t} + \tfrac{1}{2}\mathcal{E}^*(t)\mathrm{e}^{\mathrm{i}\omega t} \right] d_{ab}
\end{aligned}
\tag{2.36}
$$

where $d_{ab}$ is then the matrix element of the electric dipole operator $\mathbf{d}$ projected on the polarisation direction of the electric field. The crux of the problem is then in calculating (or looking up) dipole matrix elements for the eigenstates of a given system.

### 2.4.3 Dipole Matrix Elements and Parity

We can show that the diagonal matrix elements of $\mathbf{d} = e\mathbf{r}$ are zero by making a parity argument. We define the parity operator $\Pi$ as the unitary operator (i.e. $\Pi^\dagger \Pi = 1$) that flips the sign of the position operator $\mathbf{r}$ via

$$
\Pi \mathbf{r} \Pi^\dagger = -\mathbf{r}. \tag{2.37}
$$

Operating with $\Pi$ on the right of both sides shows that the anticommutator $\{\Pi, \mathbf{r}\} = \Pi \mathbf{r} + \mathbf{r}\Pi = 0$ and thus the matrix elements vanish

$$
\langle i| \{\Pi, \mathbf{r}\} |j\rangle = \langle i| \Pi \mathbf{r} + \mathbf{r}\Pi |j\rangle = 0 \tag{2.38}
$$

for any states $|i\rangle, |j\rangle$. Now $\Pi$ commutes with $\mathcal{H}$, and so has the same eigenstates, so we have eigenvalues $\pi_i, \pi_j$ such that $\Pi |i\rangle = \pi_i |i\rangle$ and $\Pi |j\rangle = \pi_j |j\rangle$. Thus we can write

$$
\langle i| \Pi \mathbf{r} + \mathbf{r}\Pi |j\rangle = (\pi_i + \pi_j) \langle i| \mathbf{r} |j\rangle. \tag{2.39}
$$

The right hand side can only be zero if $\pi_i + \pi_j$ is zero or if the matrix element is. Now, as $\Pi^2 = 1$, the eigenvalues $\pi = \pm 1$. So for the diagonal matrix elements, $\pi_i + \pi_i$ can't be zero and $\pi_j + \pi_j$ can't be zero so it must be that $\langle i| \mathbf{r} |i\rangle = \langle j| \mathbf{r} |j\rangle = 0$. The off-diagonal matrix elements $\langle i| \mathbf{r} |j\rangle$ are non- vanishing if the states have opposite parity such that $\pi_i = -\pi_j$.

## 2.4.4   Atomic Coherence and Polarisation

We introduced the polarisation $P$ in section 2.2 as the cumulative effect of charge separation induced on individual atoms and defined it in 2.3 as the dipole moment per unit volume. In terms of atomic observables, the polarisation at a distance $z$ through the medium at time $t$ may therefore be written as the expectation value of the scalar dipole operator for those atoms

$$P(z,t) = N(z)\langle \mathrm{d}(z,t)\rangle \tag{2.40}$$

where $N(z)$ is the number density (atoms per unit volume) of the medium, which may in general be a function of propagation distance $z$, for example in an atom cloud shaped by the geometry of a magneto-optical trap,[11] or constant for a thermal cell in thermal equilibrium.

The expectation value of an observable for a system in a pure or mixed state represented by a density matrix $\rho$ is defined in equation (A.5), such that we may write

$$P(z,t) = N(z)\,\mathrm{Tr}\,[\rho \mathrm{d}(z,t)]. \tag{2.41}$$

As we know from the above parity argument that the diagonal matrix elements of the dipole operator are zero, we may then write $P$ directly in terms of the off-diagonal elements and the atomic coherences, via

$$P(z,t) = N(z)\sum_{i \neq j}\left[d_{ij}\rho_{ij}(z,t) + d_{ji}\rho_{ji}(z,t)\right]. \tag{2.42}$$

Now in order to relate this to the slowly-varying envelope $\mathcal{P}$, we need to rotate the density matrix elements, via

$$\rho_{ij} = \tilde{\rho}_{ij}\,\mathrm{e}^{\mathrm{i}(kz-\omega t)}$$

$$\rho_{ji} = \rho_{ij}^* = \tilde{\rho}_{ij}^*\,\mathrm{e}^{-\mathrm{i}(kz-\omega t)}$$

where tilde-notated variables $\tilde{\rho}_{ij}$ are slowly-varying density matrix elements. Dropping the tilde notation, we then derive an expression for the

slowly-varying polarisation envelope in terms of the atomic coherences

$$\mathcal{P}(z,t) = N(z) \sum_{i \neq j} d_{ij} \rho_{ij}(z,t) \tag{2.43}$$

which we may substitute into the propagation equation (2.13).

Note that in our discussion of polarisation in this section we have made no reference to the susceptibilities $\chi^{(j)}(t)$. These are implicit in the density matrix coherences. This analysis is valid for any general nonlinear form of polarisation as expressed in equation (2.15) if we can determine the evolution of atomic states from the Lindblad equation (2.29).

### 2.4.5   *Thermal Atoms*

The above analysis for the atom-light interaction is appropriate for stationary (*i.e.* ultracold) atoms but must be modified for thermal atoms due to the averaging effect of atomic motion.[12]

An atom moving with a velocity component $v$ in the $z$-direction will interact with a Doppler-shifted field frequency $\omega - kv$. This shift is effected over a 1D Maxwell-Boltzmann probability distribution function of velocity[13,14]

$$f(v) = \frac{1}{u\sqrt{\pi}} e^{-(kv/u)^2} \tag{2.44}$$

where the thermal width $u = kv_w$. Here $k$ is again the wavenumber of the quasi-monochromatic field and $v_w = 2k_BT/m$ is the most probable speed of the Maxwell-Boltzmann distribution for a temperature $T$ and atomic mass $m$. As is usual, $k_B$ represents the Boltzmann constant.

To include this Doppler effect in the field propagation equations (2.13), we replace the atomic coherence factor by an integral over a convolution of $f(v)$, with the atomic coherence now a function of velocity, so that

$$\mathcal{P}(z,t) = N \sum_{i \neq j} d_{ij} \int_{-\infty}^{\infty} \rho_{ij}(z,t;v) f(v) \mathrm{d}v. \tag{2.45}$$

This velocity-dependent $\rho_{ij}(z, t; v)$ represents the atomic coherence resulting from interaction with a field at the Doppler-shifted frequency $\omega - kv$.

The result of the inclusion of thermal effects is a broadening of absorption resonance widths, a familiar concern in spectroscopy. We will consider example spectral profiles in section 2.5.

### 2.4.6 *Shifting to the Speed-of-Light Reference Frame*

To solve the propagation equation (2.13) as a boundary value problem, it is useful to introduce co-moving variables $\zeta = z$ and $t' = t - z/c$. This is equivalent to using a reference frame that moves with the speed of light across the medium.[12] We then have

$$\frac{\partial}{\partial \zeta} = \frac{\partial z}{\partial \zeta}\frac{\partial}{\partial z} + \frac{\partial t}{\partial \zeta}\frac{\partial}{\partial t} = \frac{\partial}{\partial z} + \frac{1}{c}\frac{\partial}{\partial t} \tag{2.46}$$

so that

$$\frac{\partial}{\partial z}\mathcal{E}(z, t') = i\frac{k}{2\epsilon_0}N(z)\sum_{i \neq j} d_{ij}\int_{-\infty}^{\infty}\rho_{ij}(z, t; v)f(v)\mathrm{d}v. \tag{2.47}$$

In this reference frame we see that the propagation equation for the field is now a differential equation only in $z$.

### 2.4.7 *A Recap*

At this point we have derived a set of coupled partial differential equations describing the dynamics of the atomic density operator (2.29) and the propagation of the electric field envelope (2.47).

These coupled equations can be integrated numerically for a given set of boundary conditions defining the input profile of the electric field and the initial state of the atoms. The integration proceeds via the following recipe, which must be repeated in a self-consistent manner:

1. Solve the Lindblad master equation for the quantal dynamics of the atomic density matrix over time $t'$.

2. Average the Maxwell-Boltzmann probability distribution over velocity $v$.

3. Solve the Maxwell wave equations for propagation of the electromagnetic field over space $z$.

The description of the specific numerical algorithms used for integration, along with details of the Python code used to implement these algorithms, is given in appendices B and C. We will make use of these methods to solve the MB equations for various systems of interest throughout the chapters of this thesis.

## 2.5   *Linear Propagation in Two-level Atoms*

Now that we have derived the necessary differential equations to describe 1D propagation in an atomic vapour and described computational algorithms for the numerical solution of the problem for a given set of boundary conditions, we will look at example results from simulated propagation of a monochromatic (*i.e.* single carrier frequency) field in a simple two-level system.

We will define the two-level system and present the results of propagation for some boundary conditions representative of laboratory experiments: pulsed and continuous-wave (CW) input fields. We'll then make an analysis of the frequency dependent behaviour of the simulated propagation of a wider-spectrum field. We will use these results to verify that these results match the known analytic response functions for the linear regime, such that we have confidence in the computational

scheme for the simulations we will later obtain for nonlinear systems with more than one carrier frequency.

We will also introduce the natural unit system which will be used throughout this thesis.

### 2.5.1 The Two-level System

No real atomic system exists with only two levels of course, but this minimal scheme is a good approximation in the case of resonant interaction with a well-separated transition.

The system is defined by a Hilbert space covered by a basis that consists of a ground state $|0\rangle$ and an excited state $|1\rangle$ with eigenenergies $E_0$ and $E_1$. The resonance frequency $\omega_0 = (E_1 - E_0)/\hbar$. As is conventional we define the detuning of the input carrier frequency from resonance as $\Delta = \omega - \omega_0$ and the complex Rabi frequency[15]

$$\Omega(z,t) = \frac{d_{01}}{\hbar}\mathcal{E}(z,t) \tag{2.48}$$

where $d_{01} = \langle 0|\, d\, |1\rangle$ is the transition dipole matrix element.

The time evolution is independent of the absolute value of the bare state energies, so we may set the ground state energy $E_0 = 0$. Making the rotating wave approximation, we find that the atomic Hamiltonian is given by

$$\mathcal{H} = \hbar \begin{bmatrix} 0 & \Omega/2 \\ \Omega^*/2 & -\Delta \end{bmatrix} \tag{2.49}$$

in the frame rotating with the carrier frequency.[16]

For the Lindblad superoperator $\mathcal{L}$ we have just a single collapse operator representing spontaneous decay of the electron from the the excited state to the ground state

$$C = \sqrt{\Gamma}\,|0\rangle\langle 1|\,. \tag{2.50}$$

In two-level medium we only have one dipole matrix element and one coherence to consider, such that (neglecting the Doppler effect for now) the propagation equation (2.47) may be written

$$\frac{\partial}{\partial z}\mathcal{E}(z,t') = iN(z)\frac{k}{2\varepsilon_0}d_{01} \cdot \rho_{01}(z,t'). \qquad (2.51)$$

It is useful to write the propagation now in terms of the Rabi frequency

$$\frac{\partial}{\partial z}\Omega(z,t') = iN(z)g \cdot \rho_{01}(z,t') \qquad (2.52)$$

where we define a propagation coefficient

$$g_{01} = \frac{d_{01}^2 k}{2\varepsilon_0 \hbar} \qquad (2.53)$$

which is constant for a given transition with dipole matrix element $d_{01}$ and for a field with carrier wavenumber $k$.

### 2.5.2  The Natural Unit System

For a two-level system we have a single natural linewidth, and so it is convenient to introduce a natural unit system, with frequencies in units of the natural linewidth $\Gamma$, times in terms of the reciprocal spontaneous decay lifetime $\tau = 1/\Gamma$ and distances in terms of the length of the medium $L$.

To give an illustrative example, we will take a rubidium 85 cell and apply a monochromatic field on resonance with the D1 transition from the $5^2S_{1/2}$ ground state to the $5^2P_{1/2}$ excited state at $\omega = 2\pi \times 377\,\text{THz}$. The spontaneous decay rate for the transition $\Gamma = 2\pi \times 5.75\,\text{MHz}$ such that the lifetime $\tau = 27.6\,\text{ns}$. The transition dipole matrix element is $d_{01} = 2.53 \cdot 10^{-29}\,\text{C m}$. From this we can calculate that the propagation coefficient for the transition $g_{01} = 2\pi \times 4.34 \cdot 10^{-9}\,\text{MHz cm}^2$.

The number density $N$ in a contained cell is a function of the temperature of the cell. For an example temperature $T = 200\,\text{C}$ we have $N =$

$9.26 \cdot 10^{14} \, \mathrm{cm}^{-3}$. If we then take a cell of a typical length $L = 1 \, \mathrm{mm}$, the key parameter we require for describing propagation in the medium can be expressed purely in terms of the natural units as $N g_{01} = 2\pi \times 70 \, \Gamma / L$.

By introducing this natural unit system we are able to reduce the number of parameters involved in the mathematical problem. For example, it becomes clear that increasing the length of the medium ten times is equivalent to raising the number density by the same scale, or by choosing a system with a suitably higher dipole moment.

### 2.5.3  Weak Probe Lineshape

The Lindblad master equation (2.29) represents a set of differential equations in time for the time evolution of each density matrix element.

As we know via equation (2.43) that the polarisation $\mathcal{P}$ is related to the off-diagonal coherence $\rho_{01}$, we write out the particular equation to follow its time evolution, such that

$$\frac{\mathrm{d}\rho}{\mathrm{d}t} = \mathrm{i}\Omega \left( \rho_{00} - \rho_{11} \right) + \left( \mathrm{i}\Delta - \frac{\Gamma}{2} \right) \rho_{10}. \tag{2.54}$$

In the case of weak field input on the medium, we may assume that we're in a quasi-static regime where the atomic density matrix changes negligibly over the time of the input. We thus set the time derivative in equation (2.54) to zero.

The initial condition is that all of the atomic population starts in the ground state. For a weak field we may also assume that population transfer is negligible such that $\rho_{11} = 0$.

Under these weak field approximations, we may thus derive the steady state, weak field lineshape

$$\rho_{01}(z) = -\Omega(z) \frac{1}{\mathrm{i}\frac{\Gamma}{2} + \Delta}. \tag{2.55}$$

### 2.5.4 Weak Pulse Propagation Results

The first Maxwell-Bloch simulation results we will consider are for an input field profile of finite duration, namely a Gaussian pulse. In general for short duration pulses, the atoms do not reach equilibrium with the applied field before the pulse has passed, however for weak fields so little population is transferred that a quasi-static regime can be a good approximation.

The Gaussian pulsed input field is defined by

$$\Omega(t) = \Omega_0 \exp\left[-4\log 2 \left(\frac{t - t_0}{t_w}\right)\right] \tag{2.56}$$

where $\Omega_0$ is the peak input Rabi frequency, $t_0$ is the time at which the function reaches that peak, and $t_w$ is the full width at half maximum (FWHM) of the pulse.

In this simulation we let the peak $\Omega_0 = 2\pi \times 10^{-3}\,\Gamma$, the centre $t_0 = 0$ and the width $t_w = 0.1\,\tau$. We define the medium to have a length $L$, number density $N$ and coupling $g$ such that the key absorption parameter $Ng = 2\pi \times 1\,\Gamma/L$.

In figure 2.1 we present a colour map of the simulated real part of the complex Rabi frequency $\Omega(z, t)$ describing the field profile as it propagates through the medium.

Time $t$ is shown on the $x$-axis and the propagation distance $z$ is shown on the $y$-axis such that the field enters at the bottom of the plot. The horizontal slice at $z = 0$ thus represents the Gaussian input field. All propagation results are presented in the speed-of-light reference frame described in section 2.4.

We see that the primary pulse envelope is attenuated and slightly fast, such that the first peak arrives at the rear of the medium, $z = 1\,L$, at a time $t \approx -0.05\,\tau$ in the speed-of-light reference frame. [normal disper-
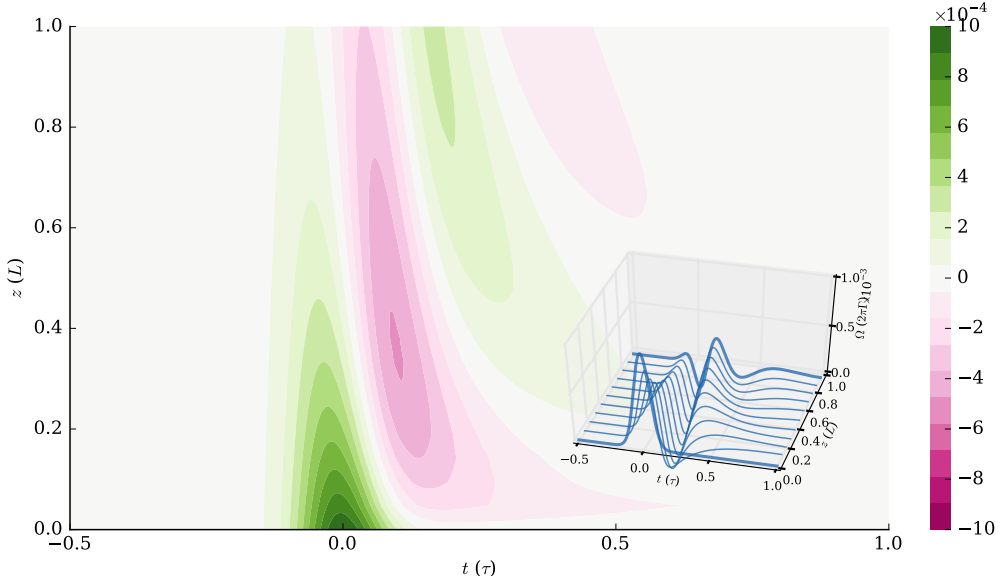
FIGURE 2.1 The real part of the complex Rabi frequency $\Omega(z, t)$ showing the simulated result of propagation of a weak pulse through a two-level medium. (Inset 3D) The field has Gaussian profile entering the medium at $z = 0$, with peak $\Omega_0 = 2\pi \times 10^{-3}\,\Gamma$ and width $t_w = 0.1\,\tau$.

sion profile]. Not all of the energy of the pulse is absorbed, however. This is because the pulse is short in duration relative to $\tau$, such that its spectral profile is wider in frequency space than the absorption window of the atoms. Thus some spectral components of the field see a medium which is transparent to them. However, they remain subject to phase shift. We see high-frequency ringing, also described as a $0\pi$ pulse as the total area integrates to zero.[16,17]

In figure 2.2 we present colour maps of simulated density matrix elements describing the response of the atoms along the medium as the applied field reaches them.

The cumulative Rabi frequency of the pulse is many orders of magnitude too small to saturate the excited state population so that for the atoms at the front of the medium at $z = 0$, $\rho_{11}$ continues to rise through the pulse to a peak at time $t \approx 0.01\,\tau$ after the input field has peaked. There is a small 'echo' in the excited state, due to the field ringing, visi-
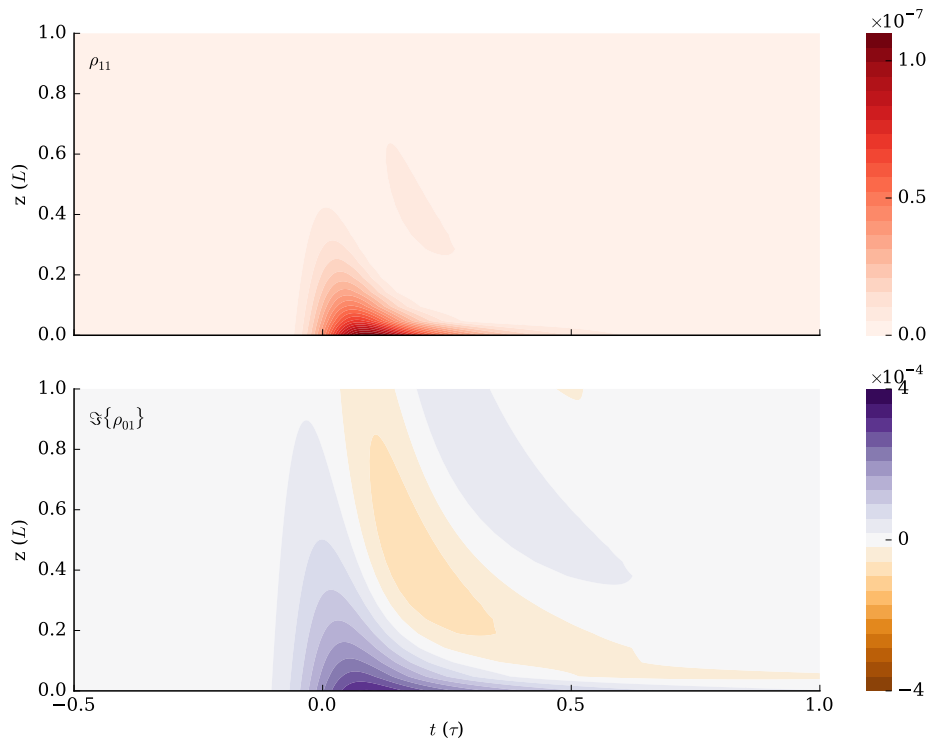
FIGURE 2.2  Density matrix elements of the two-level atom system as a function of $z$ and $t$ during the simulation. (Top) Excited state population $\rho_{11}(z, t)$. (Bottom) Coherence $\rho_{01}(z, t)$ between the states. The simulation parameters and boundary conditions are as for figure 2.1.

ble at $t \approx 0.2\,\tau$ and between $z = 0.4\,$L and $0.6\,$L.

A positive imaginary coherence $\Im[\rho_{01}]$ is driven by the applied field at the front of the medium. We observe that the coherence decays at half the rate of the excited state population, $\Gamma/2$, consistent with equation (2.54).

### 2.5.5 Spectral Analysis

In section 2.3 we made use of Fourier transforms to shift perspective to the frequency domain. We showed that in the linear regime it is possible to derive a response function, given in equation (2.22), which when substituted into the propagation equation allows us to understand how the susceptibility describes the frequency-dependent absorptive and dispersive properties of a medium with respect to a weak field.

In order to verify the numerical model we have developed, as well as to demonstrate these spectral properties, we will now look at results from a simulation of a pulse propagating through the two-level medium. We wish to confirm that the results of the simulation match the known analytic response functions for the linear regime.

For this simulation we define an unusual and artificial time profile for the input field boundary condition: a cardinal sine (sinc) function given by

$$\Omega(t) = \frac{1}{20\sqrt{2\pi}}\mathrm{sinc}(10t). \tag{2.57}$$

This input profile, shown in the top subplot of figure 2.3, is clearly impractical for any experimental setup. We choose this profile because its Fourier transform, shown in the bottom subplot of figure 2.3, is a square function with a width of $10\,\Gamma$. This gives us a wide spectral range over which to observe the effect of the two-level medium on the field.
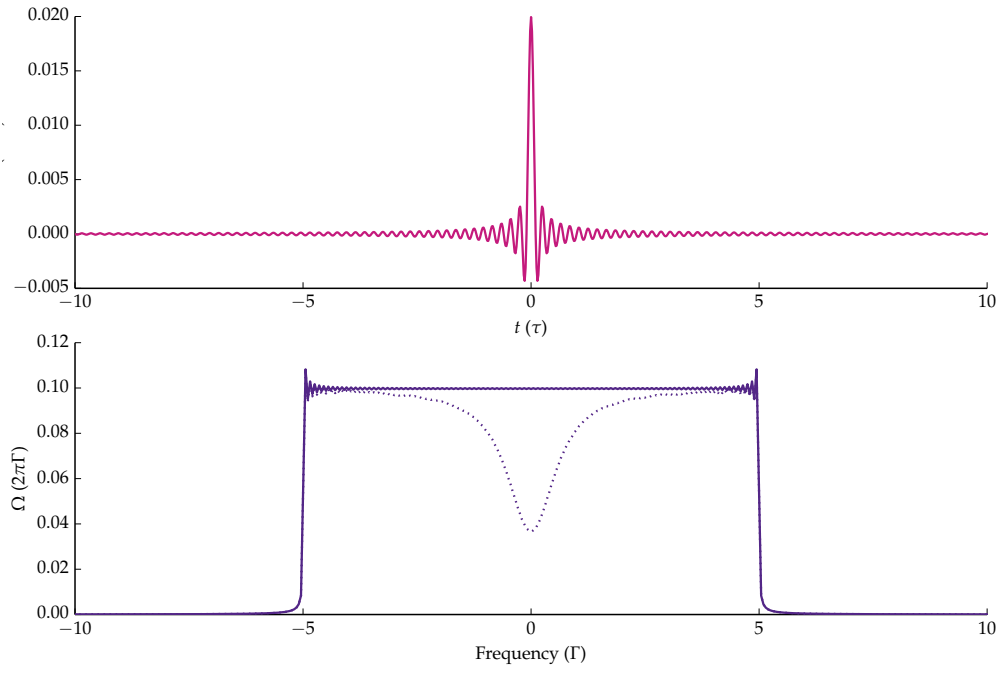
FIGURE 2.3   (Top) The sinc function (pink) defined by equation (2.57) which forms a simulated pulse profile in time $\Omega(t, 0)$ entering the medium at $z = 0$, *i.e.* the boundary condition. (Bottom) (Purple solid) The discrete Fourier transform $|\Omega(\omega, 0)|$ of the sinc shape above, representing the same function in the frequency domain at $z = 0$. (Purple dotted) The resulting field profile $|\Omega(\omega, z = 1)|$ in the frequency domain at $z = 1\,\mathrm{L}$, after propagation through the medium. The medium is defined with a length $L$, number density $N$ and coupling $g$ such that $Ng = 2\pi\,1\,\Gamma/\mathrm{L}$.
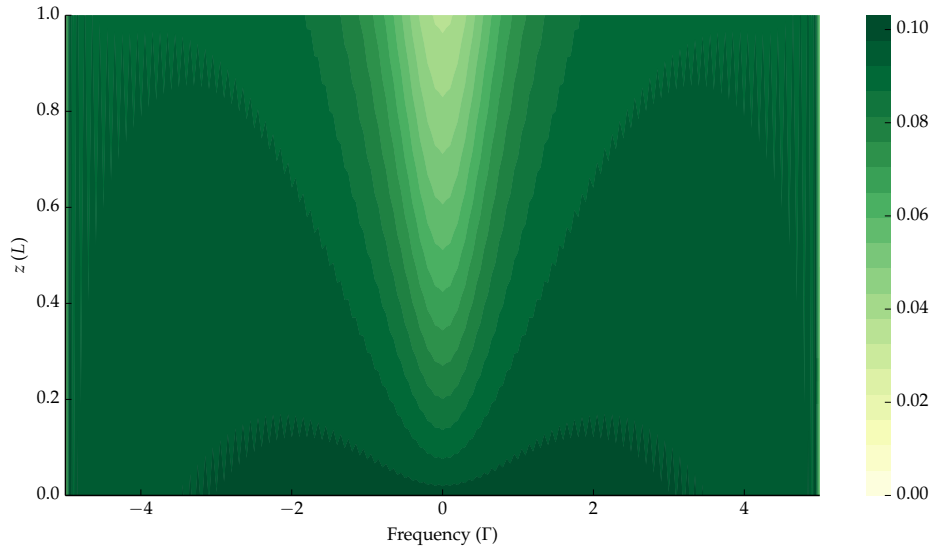
FIGURE 2.4 Magnitude of the Fourier-transformed Rabi frequency $|\Omega(z,\omega)|$, showing propagation of the field through the medium in the frequency domain during the simulation. The input boundary condition field profile at $z = 0$ is the sinc function shown in figure 2.3. The medium is defined with a length $L$ and number density $N$ such that $Ng = 2\pi\,1\,\Gamma/L$.

The discrete Fourier transform (DFT) is used as the numerical method for shifting to the frequency domain, which results in some Gibbs ringing[18] seen at the corners at $\pm 5\,\Gamma$.

A more-realistic Gaussian time profile, short in duration, would also cover a wide spectral range. We choose the sinc function for the reason that it provides greater accuracy in the wings far away from resonance, where both the input and output field amplitudes would be extremely small for the Gaussian function, bringing inaccuracy as we get close to limits for floating point storage.

The absorptive effect of the medium is immediately visible if we compare the $|\Omega(\omega, z{=}1)|$, the profile at the back of the medium, also shown (dotted) in the bottom subplot of figure 2.3. Around resonance there is a significant dip of around 60% in the transmitted Rabi frequency (and thus the electric field amplitude).

In figure 2.4 we show the results for $|\Omega(\omega, z)|$ as the sinc pulse moves through the medium. On resonance, the field decays exponentially while in the spectral wings we see nearly full transmission.

We can compare the simulated result with the analytic expression given in equation (2.25), which tells us that we can obtain the imaginary part of the susceptibility by checking the attenuation of the field via

$$\frac{k}{2}\chi_I(\omega)z = -\log\frac{|\Omega(z,\omega)|}{|\Omega(z=0,\omega)|} \tag{2.58}$$

and the real part of the susceptibility by checking the phase shift over the medium,

$$\frac{k}{2}\chi_I(\omega)z = \phi(z,\omega) - \phi(z=0,\omega) \tag{2.59}$$

where the $\phi$ is defined via

$$\Omega(z,\omega) = |\Omega|e^{i\phi}. \tag{2.60}$$

In figure 2.5 we present the simulated results for the susceptibility as defined in (2.58) and (2.59).

We see that the imaginary part, describing absorption of the field, has the Lorentzian lineshape familiar as a solution for classical systems involving forced and damped resonance. The FWHM is measured numerically, and as we would expect it is equal to $1\Gamma$, the natural linewidth around which we designed the natural unit system.

Absorption linewidths observed in experiment will in general be significantly wider, as the important effects of Doppler broadening and atomic collisions must be considered. This natural linewidth represents the theoretical minimum linewidth that could be observed for cold atoms due to spontanous emission rate, which for an atom in free space can never be reduced.[15]

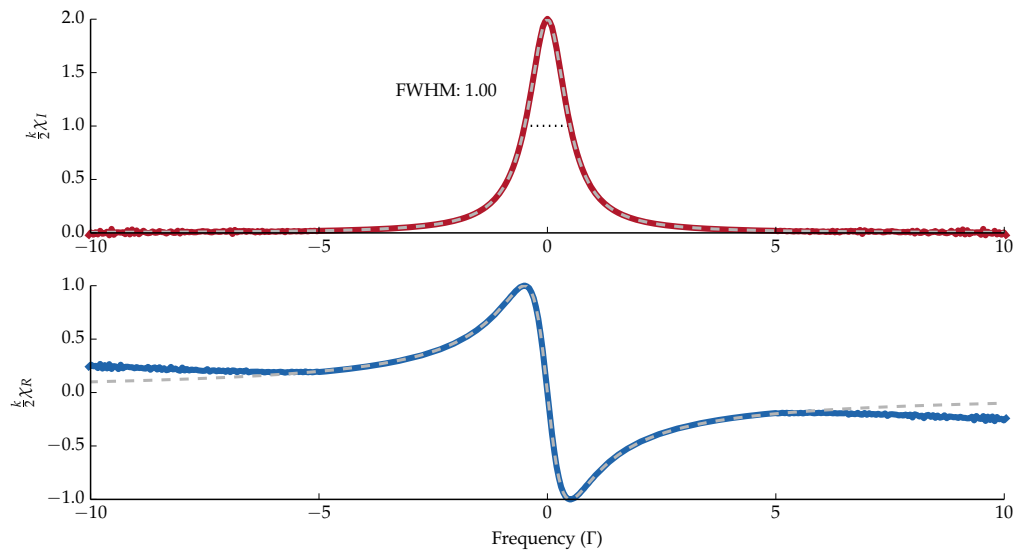The real component has the familiar dispersion lineshape describing the

FIGURE 2.5 (Top) (red solid) The imaginary part of the linear susceptibility $\chi_I$ derived from the simulation via equation (2.58). (Bottom) (blue solid) The real part of the linear susceptibility $\chi_R$ derived from the simulation via equation (2.59). (grey dashed) Analytic functions of $\chi_I$ and $\chi_R$ derived from the weak probe lineshape given in equation (2.61). The FWHM of the $\chi_I$ lineshape is shown as measured numerically.

phase of the input field relative to the frequency of the oscillator as it passes over resonance from lagging to leading.[3]

By comparing the linear propagation equation (2.23) with the weak probe approximation for the coherence, given in equation (2.55), we note that we can also derive an analytic expression for the frequency-dependent susceptibility in this regime,

$$\frac{k}{2}\chi(\omega) = -Ng\frac{1}{i\frac{\Gamma}{2} + \Delta}. \tag{2.61}$$

The real and imaginary parts of this function are overlaid (grey dashed lines) on the simulated results and we see excellent agreement around resonance. We see in (2.61) that the imaginary part of the susceptibility, and thus the absorption, is solely due to the spontaneous decay term $\Gamma$. This we can understand as it is this scattering of energy by the atoms to the environment which results in a loss of energy in the system.

Spectral field components beyond $\pm 5\Gamma$ are negligible (as defined by the sinc function, see figure 2.3) and so we see some noise in the result beyond this point. We also see deviation between the analytic and simulated results in the dispersion profile far from resonance, which is due to the linear susceptibility approximation being valid only for near-resonant components of the field.

This result tells us that the computational scheme designed to model propagation of light in atomic media is accurate in the linear regime, which gives us confidence in the scheme for the work we will do later going beyond this weak field limit.

In the scope of input field boundary conditions, at the other extreme to short duration, wide-spectral pulses are continuous wave (cw) fields, with constant intensity over time. Such field envelopes are monochromatic, meaning that the frequency domain representation of a cw field in the time domain is a Dirac delta function.
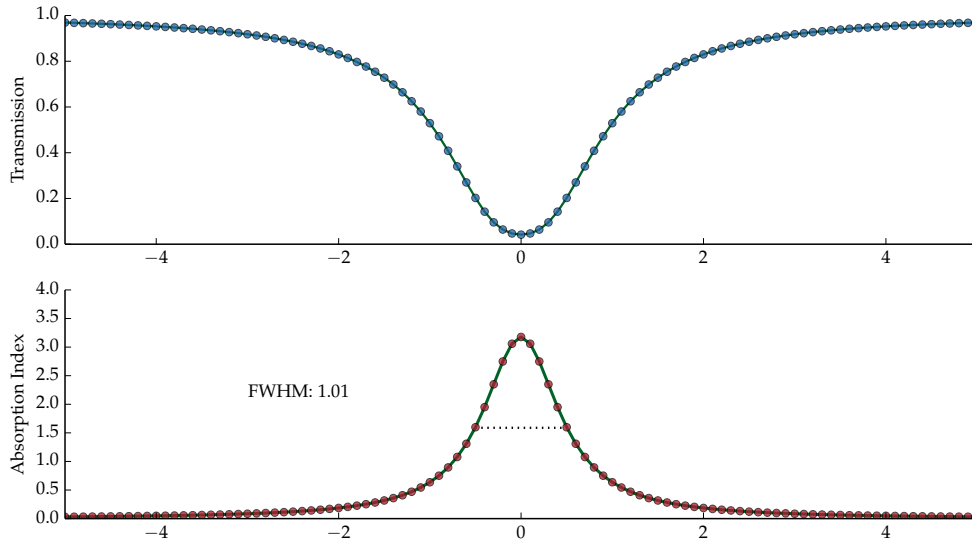
FIGURE 2.6   Peak transmission (top) and absoptive index (bottom) for a monochro-
matic cw field across a discrete range of 100 detunings Δ around reso-
nance. The solid lines in both represent the same values for the continu-
ous spectrum deriving from propagation of the short sinc pulse function.

In figure 2.6 we make a scan of the field detuning Δ across resonance
with the two-level atom, and mark the peak transmission ($T = I/I_0$) of
the field along with the associated absorptive index.

We also plot the transmission and absorption index of the transmission
and absoprtion as a function of frequency for the wide-spectrum sinc
pulse. The close agreement tells us that the short pulse's propagation is
as if it were composed of many monochromatic frequency components
interacting independently with the medium. In the linear regime, the
solution is a superposition of individual frequencies.[2]

## 2.5.6   *The Voigt Profile*

As mentioned, the lineshapes presented thus far for weak probe spectra
neglect the thermal motion of the atoms, and so are only valid for atoms
that are stationary, *i.e.* close to absolute zero.

To account for thermal atoms, we must include the Doppler effect by means of the average over detunings described by the integral in equation 2.45. The thermal lineshape function may then be expressed as

$$s(\Delta) = \int_{-\infty}^{\infty} h(\Delta - kv) \times f(\Delta)\mathrm{d}v \tag{2.62}$$

where the weak probe natural lineshape

$$h(\Delta) = -Ng\frac{1}{i\frac{\Gamma}{2} + \Delta} \tag{2.63}$$

is given in equation (2.61) and $f(v)$ is the Maxwell- Boltzmann distribution over atomic velocities $v$ given in equation (2.44).

Using the convolution theorem for Fourier transforms, this integral can be computed as

$$s(\Delta) = \frac{i\sqrt{\pi}}{2u}e^{-z^2} \times \mathrm{erfc}(-iz) \tag{2.64}$$

where $z = ia/2 + b$ given $a = \Gamma/u$ and $b = \Delta/u$, and *erfc* is the complementary error function.[19] This convolution of a Lorentzian function with a Gaussian function is known as a Voigt profile.

In figure we show simulated results for the real and imaginary parts of the susceptibility for the same system as in figure 2.5, but this time including Doppler effects in the numerical algorithm by a weighted averaging over a range of velocity classes as described in appendix C. We take the thermal width to be $u = 2\pi \times 0.5\,\Gamma$. As an example, this might correspond to a $\sim 0.1\,\mathrm{mK}$ vapour of $^{85}$Rb probed on the D1 line.

We compare these simulated lineshapes with the weak probe Voigt profile given in equation (2.64) and see agreement with the analytic result. We see that the inclusion of temperature in the model has the effect of broadening the spectral lineshapes.
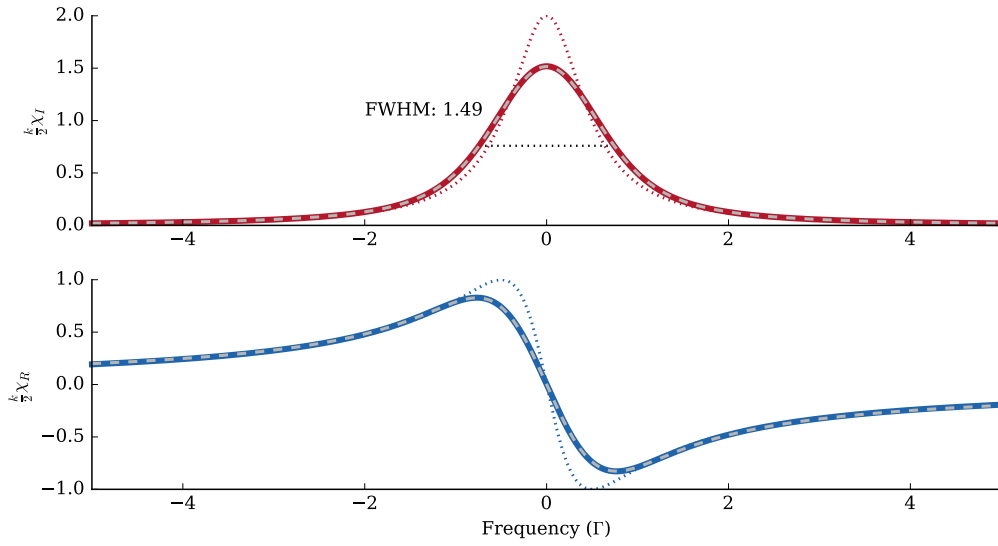
FIGURE 2.7    Top) The imaginary part of the linear susceptibility $\chi_I$ derived from a thermal simulation via equation (2.58). (Bottom) (blue solid) The real part of the linear susceptibility $\chi_R$ derived via equation (2.59). (grey dashed) Analytic functions of $\chi_I$ and $\chi_R$ derived from the convoluted Voigt profile given in equation (2.64).

## 2.6    Discussion

In this chapter we started from the Maxwell equations and derived a propagation equation for monochromatic light, using the slowly varying envelope approximation. We introduced the linear and nonlinear optics, and for the linear regime, for weak fields, the useful concept of susceptibility and how this relates to the absorptive and dispersive response of the medium.

Going beyond the linear regime, we need to follow the quantal dynamics of the atomic density matrix, which we do with the Lindblad master equation. We defined the interaction Hamiltonian within the electric dipole approximation, and how the polarisation of the medium can be derived from atomic coherences. For thermal atoms this coherence must be averaged over a Maxwell-Boltzmann distribution. We discussed algo-

rithms (presented in appendix C) for integrating the propagation equations numerically for nonlinear propagation.

We presented results for a two-level system in the linear regime. In doing so we used spectral analysis to compare with the analytic results derived in this regime. The good agreement in these results gives us confidence in the numerical methods. In the next chapter, we will employ the model in considering nonlinear pulse propagation in two-level and three-level systems.

# 3    Nonlinear Propagation Phenomena

# 4   *Storage and Retrieval of Dark-State Polaritons*

# 5 Two-Photon Excitation in a High-Intensity Beam

# 6  Propagation of Short Pulses in V-type Atoms

# 7 Conclusions

# A    Dynamics of Open

# Quantum Systems

## A.1    The Density Operator

We typically describe the state of a quantised atomic system via its state
vector

$$|\psi\rangle = \sum_j c_j |j\rangle \,, \tag{A.1}$$

a linear superposition of the eigenstates $|j\rangle$. There are many physical
situations, however, in which there is significant coupling to an external
environment the state evolution of which we cannot follow.

Atom-light interactions are one such system. While the processed of ab-
sorption and stimulated emission (of photons from and to the applied
field) can be described within a *closed quantum system*, the process of
spontaneous decay due to interaction with vacuum fluctuations sur-
rounding an atom cannot.

For such *open quantum systems* it is useful to generalise the concept of
$|\psi\rangle$ to that of the *density operator* $\rho$. A *pure state* is one that can be repre-
sented by a linear superposition as in (A.1), for which the density matrix
is defined as $\rho = |\psi\rangle \langle\psi|$. This is clearly equivalent in information to $|\psi\rangle$.
The usefulness of the density operator $\rho$ is that it can be generalised in a

statistical way to represent incoherent superpositions of wavefunctions. We assume we have a mixture of states $|\psi_s\rangle$ each with different expansions in the eigenbasis $|j\rangle$, contained in the ensemble with probabilities $P(s) \geq 0$. The density operator for this general *mixed state* is then defined as

$$\rho = \sum_s P(s) |\psi_s\rangle \langle\psi_s| \tag{A.2}$$

where for proper normalisation

$$\sum_s P(s) = 1. \tag{A.3}$$

We may consider that $|\psi\rangle$ describes the intrinsic Heisenberg uncertainty required by quantum mechanics, where $\rho$ is also able to describe additional uncertainty representing our state of knowledge of the system.[20]

The matrix representation of the density operator in a particular basis is also known as the density matrix. The off-diagonal elements $\rho_{jk} = \langle j| \rho |k\rangle$ depend on relative phase of the coefficients and are known as *coherences*. The diagonal matrix elements $\rho_{jj} = \langle j| \rho |j\rangle$ represent the probability of a measurement finding the system in state $|j\rangle$ and are known as *populations*. These populations form a probability distribution and so must be normalised such that

$$\mathrm{Tr}\,[\rho] = \sum_j \rho_{jj} = 1. \tag{A.4}$$

The expectation value of an operator $A$ in the density matrix formalism is given by

$$\langle A \rangle = \mathrm{Tr}\,[A\rho]. \tag{A.5}$$

## A.2   The Master Equation

By substituting the density operator $\rho$ into the standard Schrödinger equation for motion of the quantum state

$$i\hbar\frac{\partial}{\partial t}\left|\psi\right\rangle = \mathcal{H}\left|\psi\right\rangle$$

we obtain the *von Neumann equation* for unitary evolution

$$i\hbar\frac{\partial\rho}{\partial t} = [\mathcal{H},\rho] \tag{A.6}$$

which for pure states is equivalent to the Schrödinger equation.

We wish to extend the formalism to mixed states and derive an equation of motion for the open quantum system interacting with an environment. The observed effect of interaction with an unmonitored environment is to introduce non-deterministic transitions between eigenstates and dephasing between them.

We start by expanding the model to include the environment, such that the total system is closed and described by (A.6). In order to meet this requirement, we must consider the Hilbert space of the total system, and a total Hamiltonian operating over that space

$$\mathcal{H}_\Sigma = \mathcal{H} + \mathcal{H}_E + \mathcal{H}_C \tag{A.7}$$

where $\mathcal{H}$ is the Hamiltonian of the system, $\mathcal{H}_E$ is the Hamiltonian of the environment, and $\mathcal{H}_C$ is the Hamiltonian describing the interaction between the system and the environment.

As we're only concerned with the dynamics of $\mathcal{H}$, we then make a partial trace over the environment degrees of freedom in (A.6) to obtain a master equation for time evolution of the system. The *Lindblad master equation* is a general, trace-preserving and positive form for the reduced density matrix $\rho$, given by

$$i\hbar\frac{\partial\rho}{\partial t} = [\mathcal{H},\rho] + \mathcal{L}\left\{\rho\right\} \tag{A.8}$$

where the Lindblad term given by

$$\mathcal{L}\{\rho\} = \sum_j C_j \rho C_j^\dagger - \tfrac{1}{2}\left(\rho C_j^\dagger C_j + C_j^\dagger C_j \rho\right) \tag{A.9}$$

is a superoperator describing the system interaction with its environment via collapse operators $C_j$ coupling states. For example, to account for a stochastic interaction with the environment representing the decay of a system from state $|k\rangle$ to state $|j\rangle$ with rate $\Gamma_{jk}$, we include a collapse operator

$$C_j = \sqrt{\Gamma_{jk}}\,|j\rangle\langle k|$$

in the Linblad term.

For the Lindblad equation (*A.8*) to be applicable as a master equation for the system, a couple of approximations must be justified. Firstly, the Born approximation requires that the environment is sufficiently large that it is not much affected by interaction with the system. We may write this as

$$\rho_\Sigma \approx \rho \otimes \rho_E. \tag{A.10}$$

Secondly, the Markov approximation requires that the time evolution depends on $\rho(t)$ and not any past history — this is also called a 'short-memory environment'.

# B Numerical Integration of the Lindblad Master Equation for Large Density Matrices

# C  Numerical Integration of the Maxwell-Bloch Equations

In this appendix we describe the design and implementation of numerical methods to solve the coupled Maxwell-Bloch (MB) equations describing the nonlinear propagation of near-resonant light through thermal atomic vapours. The derivation of the MB equations is given in chapter 2 and simulated results from the scheme here described are presented throughout the thesis.

## C.1  Formulating the Problem

The MB equations are together equations (2.47) and (2.29), which we will restate here for completeness. They are the first-order Maxwell wave equation with the slowly-varying envelope approximation

$$\frac{\partial}{\partial z}\mathcal{E}(z,t') = \mathrm{i}\frac{k}{2\epsilon_0}N(z)\sum_{i\neq j}d_{ij}\int_{-\infty}^{\infty}\rho_{ij}(z,t;v)f(v)\mathrm{d}v.$$

describing propagation of the field envelope and the Lindblad master equation

$$\mathrm{i}\hbar\frac{\partial\rho}{\partial t} = [\mathcal{H},\rho] + \mathcal{L}\{\rho\}$$

describing the time-evolution of the atomic density matrix interacting with that field.

We describe the problem in the natural unit system defined in section **??**, in terms of the length of the medium $L$, the natural linewidth of the transition $\Gamma$ (specifically the probe transition in the case of schemes with multiple field modes) and its reciprocal natural decay time $\tau = 1/\Gamma$. Our goal is to solve the MB equations over a domain in 1D space $z \in [0, 1]$ and co-moving time $t' \in [t_{\min}, t_{\max}]$.

We begin by setting up a discrete lattice over $z$ and $t'$, with $N_z$ equal spacesteps of length $h_z = 1/N_z$, such that $z_j = j \cdot h_z \; \forall j \in \{0, 1, 2, \ldots, N_z\}$ and $N_t$ equal timesteps of duration $h_t = 1/N_t$, such that $t_k = k \cdot h_t \; \forall k \in \{0, 1, 2, \ldots, N_t\}$.

The overall strategy is then to calculate values for the discretised electric field $\mathcal{E}_{j,k}$ across the lattice, for which we must determine the macroscopic polarisation $\mathcal{P}_{j,k}$ of the atoms, which in turn is derived from the density matrix $\rho_{j,k}$. A self- consistent algorithm is required for computation. Note that the electric field and polarisation envelopes in general consist of multiple modes, representing polarisations and wavelengths resonant with different transitions. For clarity in describing the scheme we will present only a single mode $\mathcal{E}_{j,k}$, but describe how the algorithm is extended to multiple modes later on.

We define a discrete set of detunings $\{\Delta_l\}$, representing atoms across a range of Doppler-shifted velocity classes. This range should be broad enough to cover the Maxwell-Boltzmann probability distribution and dense enough to accurately map the spectral absorption window. We will discuss those accuracy requirements in section C.3.

Any formulation of an integration scheme for partial differential equations is complete only with the definition of appropriate boundary conditions. Here we take a boundary condition for the field at the front of the medium (*i.e.* $j = 0$) defining the field profile over time input on the medium $\mathcal{E}_{j=0,k}$. In a typical simulation of experiment this might be a
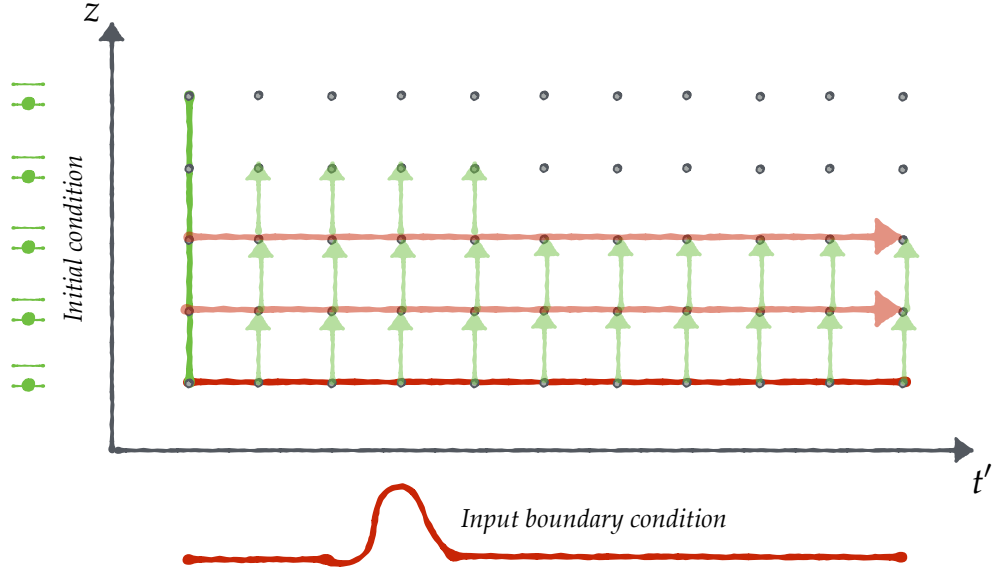
FIGURE C.1    Finite difference integration scheme for the Maxwell-Bloch equations.
The equations are solved for a discrete lattice over space $z$ and co-moving
time $t'$. At each lattice point $(z_j, t'_k)$ we wish to solve for the electric field
$\mathcal{E}(z_j, t'_k)$ and the atomic density matrix $\rho(z_j, t'_k)$. The initial condition is
illustrated by the two- level icons on the left. The boundary condition
defining the electric field pulse profile over time input on the medium is
illustrated by the sketched pulse at the bottom.

pulse or a ramp-on to a CW field. We must also specify an initial con-
dition for the density matrix $\rho_{j,k=0}$. Typically we set this such that all
population starts off in the atomic ground state.

## C.2    *Computational Scheme*

The finite difference scheme is illustrated in figure C.1 and sketched
out with pseudocode in algorithm 1. For each spacestep index $j$ in the
medium, we take the field $\mathcal{E}_{j,k}$ arriving on that step for all timesteps $t'_k$.
For the first spacestep $(j = 0)$ this is the input boundary condition, il-

---

**Algorithm 1** Maxwell-Bloch integration.

---

1: **for** $j = 2$ to $N_z$ **do**  ▷ Loop over spacesteps

2:     **for** $l = 0$ to $N_\Delta$ **do**  ▷ Loop over velocity classes

3:         $\rho_j^l = \text{solve\_lindblad}(\rho_{\text{init}}, \mathcal{E}_j, \Delta_l)$

4:     **end for**

5:     **for** $k = 0$ to $N_t$ **do**  ▷ Loop over timesteps

6:         $\mathcal{P}_{j,k} = \mathcal{N}_z \sum_{a \neq b} \int_l d_{ab} \rho_{j,k}^l [a,b] f(\Delta_l, u) \mathrm{d}\Delta$

7:         $\mathcal{E}_{j+1,k} = \mathcal{E}_{j+1,k} + \mathrm{i} h_z \frac{k}{2\varepsilon_0} \left[ \frac{3}{2} \mathcal{P}_{j,k} - \frac{1}{2} \mathcal{P}_{j-1,k} \right]$  ▷ The AB step

8:     **end for**

9: **end for**

---

lustrated in red in figure C.1. Next (lines 2–4 in the pseudocode) we loop over the velocity classes $l$ and pass the detuning $\Delta_l$, the field profile $\mathcal{E}_{j,k}$ and an initial condition ($\rho_{\text{init}}$) to the Lindblad solver described in Appendix B. That solver contains an implicit loop through the $N_t$ timesteps, and integrates the Lindblad equation to find the density matrix at each of those timesteps $t_k'$.

At this point we have solved for the density matrix $\rho_j^l$ at the spacestep $z_j$ for each time $t_k$ and for atoms in each velocity class $l$. In a loop over the timestep index $k$ (lines 5–8) we then perform an average of the density matrix coherences over detuning, weighted by the Maxwell-Boltzmann probability distribution for a defined width $u$, and sum them to find (line 6) the polarisation $\mathcal{P}_{j,k}$ at that point in space $z_j$ and time $t_k$.

Once we have computed the polarisation, and still within the loop over timesteps, we can advance the field at that timestep to the next spacestep $\mathcal{E}_{j+1,k}$ in the medium for each $k$ using a second-order Adams-Bashforth method. Note then that this method is not strictly chronological, but is self-consistent in the co-moving frame of reference.

## C.2.1   Details of the Algorithm

The pseudocode above describes the general calculation scheme, but omits a number of details that we will now describe.

First, we have considered only a single field mode. For multiple modes, we must input all of those modes to the Lindblad solver (in line 3). We must also calculate polarisations for each mode separately from its coupled transitions (line 6) and advance the fields for each mode (line 7).

Second, note that we started the spacestep loop (line 1) at $j=2$. The two-step Adams-Bashforth method requires two starting points to begin. We therefore use an explicit Euler step to take the input field at $j=0$ to the next step at $j=1$. As the local error in the Euler step is of order $\mathcal{O}(h_z)$, we use a smaller step to avoid introducing a large global error. The second step is then a two-step Adams-Bashforth with different stepsizes. The correct difference formula for this step (D.6) is derived in Appendix D. The remaining steps use the standard two-step Adams-Bashforth step as shown in the pseudocode.

Third, the Lindblad solver (line 3) requires the electric field envelope $\mathcal{E}_j$ to be passed as a function of time, rather than an array, as the adaptive method may choose different inner stepsizes (*i.e.* steps between $t'_k$ and $t'_{k+1}$ for any $k$) that we do not know in advance. We construct this function for arbitary points in the time domain using quadratic spline interpolation.[21,22]

Fourth, the complex values for the field envelopes $\mathcal{E}_{j,k}$ and atomic density matrix $\rho_{j,k}$ across the lattice is saved to disc in binary format, such that the results of each simulation can be loaded without needing the calculation to be repeated. To optimise storage and memory requirements, a data resolution in $z_h$ and $t_k$ may be specified, sufficient for analysis and visualisation without needing to record all of the steps that

may be required for stability and accuracy.

Spectral analysis of the results is performed using a discrete Fourier transform of the complex field.[21]

### C.2.2   Code Implementation

The algorithm for solving the MB equations was implemented in Python using the SciPy scientific computing stack.[23,24]

The code uses the OB class of the OpticalBloch package described in appendix B in order to define the atom-light interaction and solve the Lindblad equation for instances representing various atomic systems, with few-level or with full angular momentum structure. The QuTiP library[25] is used for quantum state and operator objects and its master equation solver for dynamics of open quantum systems.

## C.3   Convergence & Accuracy

We check the accuracy of the method with a quantitative measurement of the convergence of results for a particular system with increased number of spacesteps and velocity classes. We wish the results to be as accurate as possible, but with an awareness of the trade-off that the computational complexity (and thus running time) scales with $\mathcal{O}(N_z)$ and $\mathcal{O}(N_\Delta)$ where $N_\Delta$ is the number of velocity classes.

In figure C.2 we show the results of convergence of the integrated solutions for different numbers of spacesteps $N_z$ between 10 and 500. The convergence is measured relative to a benchmark at $10,000$ spacesteps — a number which ensures high accuracy but is too slow for performing many calculations. The maximum value of the absolute difference
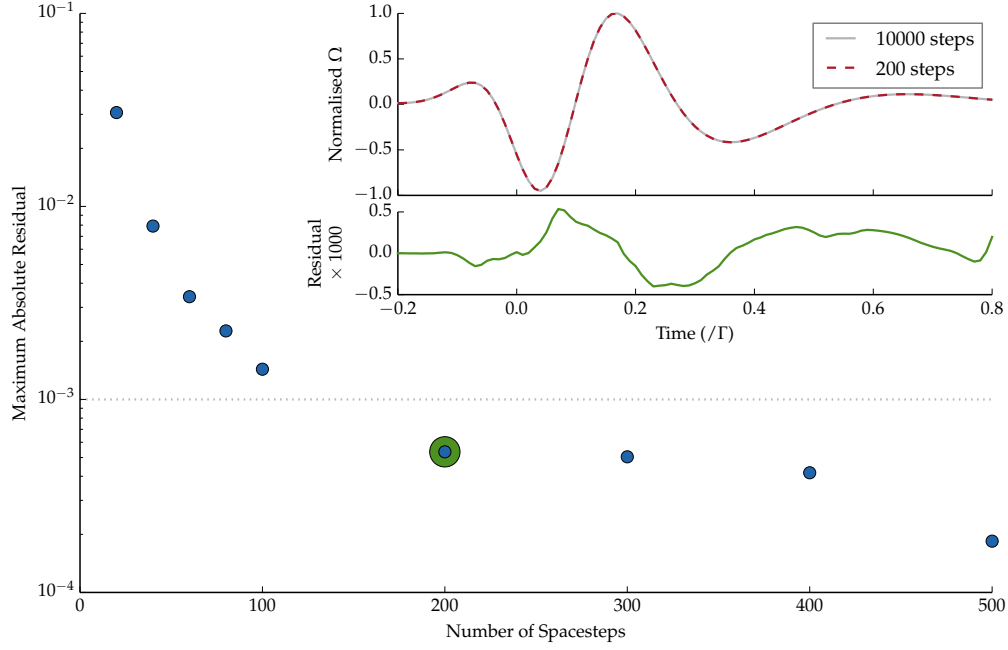
FIGURE C.2   Convergence of an example integrated solution, for a weak pulse in a medium with $\mathcal{N}g = 2\pi\,100\,\mathrm{MHz}$, for different numbers of spacesteps $N_z$. (Main plot) The minimum absolute residual between an integrated solution $N_z$ and a benchmark solution with $10,000$ steps (blue circles), plotted on a logarithmic $y$-axiz. The dotted line represents a chosen accuracy requirement of $10^{-3}$ and the green circled data point is the lowest number of steps tested which meets this requirement, in this case $N_z = 200$. (Inset) Normalised $\Omega$ against time at the final spacestep $j = N_j$ for both the benchmark and the $N_z = 200$ run, with the residual shown underneath.
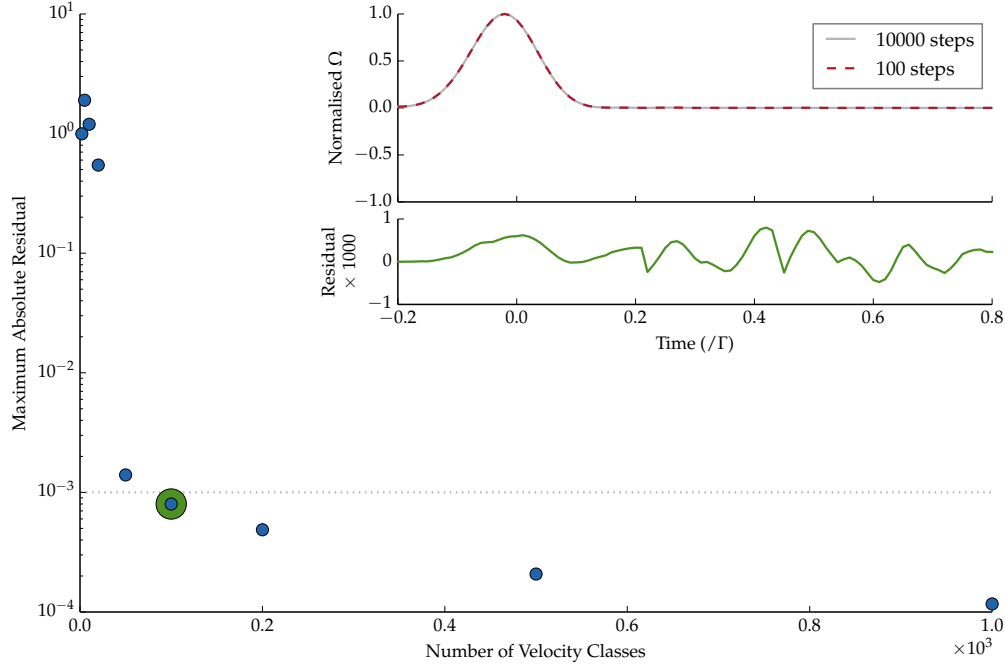
FIGURE C.3   Convergence of an example integrated solution, for a weak pulse in a medium with $\mathcal{N}g = 2\pi\,100\,\Gamma/\mathrm{L}$ and a thermal width of $2\pi\,10\,\Gamma$, for different numbers of velocity classes $N_\Delta$. (Main plot) The minimum absolute residual between an integrated solution $N_\Delta$ and a benchmark solution with $10,000$ velocity classes, plotted on a logarithmic $y$-axis. The dotted line represents a chosen accuracy requirement of $10^{-3}$ and the green circled data point is the lowest number of steps tested which meets this requirement, in this case $N_\Delta = 100$. (Inset) Normalised $\Omega$ against time at the final spacestep $j = N_j$ for both the benchmark and the $N_\Delta = 100$ run, with the residual shown underneath.

(residual) between the benchmark and each run is plotted. We see that the maximum absolute residual decreases with the number of steps $N_z$ down to 200 steps, after which the increase in accuracy for an increased number of steps is reduced. If we choose a tolerance for the maximum absolute residual of $10^{-3}$ (shown by the dotted line), the first tested run within that tolerance is $N_z = 200$. Running simulations with this number of spacesteps would therefore reduce calculation many times over the benchmark while keeping a sufficient level of accuracy.

In figure C.3 we show a similar figure for results of convergence for the integrated solutions for different numbers of velocity classes $N_\Delta$ between 1 and 1,000 spread over a width of $2\pi\, 40\,\Gamma$.

The convergence is measured relative to a benchmark at 10,000 velocity classes. We see that the maximum absolute residual is large for few velocity classes, around 1. If we again choose a tolerance for the maximum absolute residual of $10^{-3}$ (shown by the dotted line), the first tested run within that tolerance is $N_z = 100$. The 'return on investment' for additional velocity classes is reduced from then on, with $N_z = 1,000$ not providing an order of magnitude improvement in accuracy.

In picking a range of velocity classes for an accurate simulation, there are two important considerations. First, it is important to cover the Maxwell- Boltzmann distribution. We check the integration width is sufficient by using a simple trapezoidal integration over the discrete Maxwell-Boltzmann distribution to ensure it is close to unity. In each of the calculations above we used an evenly-spaced sampling over four times the FWHM. The integral is far from unity until around 20 detuning steps (when it reaches 0.995), which explains why we don't see convergence in the first few samples. Second, it is important to sample accurately the Lorentzian resonance window, which is typically much smaller than the thermal width (in our case it is specified to be $2\pi\, 1\,\Gamma$). In order to achieve both of these goals with an optimised number of detuning steps, we use a non-evenly spaced grid with a denser number of velocity classes around resonance, which can improve accuracy without requiring as many velocity classes.
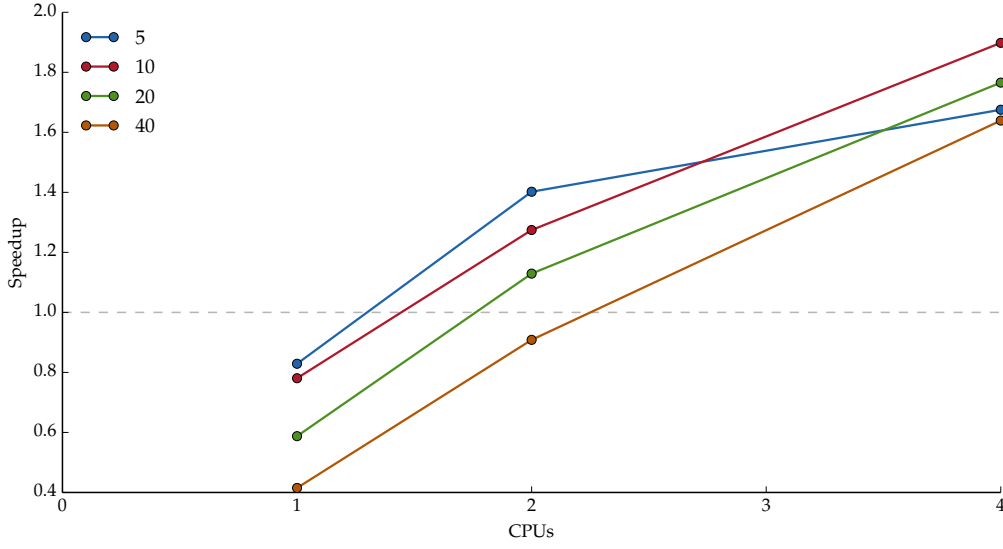
FIGURE C.4   Speedup of parallelised computation versus number of CPUs for different numbers of velocity classes $N_\Delta = \{5, 10, 20, 40\}$, relative to the serial algorithm. Each data point is 'best of two' to avoid times where the CPUs might otherwise be used by the operating system.

## C.4   *Parallelisation & Performance*

The pseudocode in algorithm 1 contains a number of nested loops, which leads us to consider if any parts of the implementation may readily be parallelised.

The iterations of the outermost loop over spacesteps $z_j$ (algorithm 1, line 1) are not independent (*i.e.* the field at a point in space $j$ is dependent on the previous space points $0, 1, \ldots, j-1$) which necessitates that these be processed in serial. However, the iterations of the inner loop over velocity classes $\Delta_l$ (algorithm 1, line 2), calculate the evolution of atoms subject to different Doppler shifts with respect to the fields along $z$. The evolution of each class is completely independent of the others so these may be processed in parallel, with the weighted average calculated at the end.

In figure C.4 we present measured speedup of parallelised computation with increasing number of CPU for example simulations using 5, 10, 20 and 40 velocity classes, relative to the serial code.

We see that, for all numbers of velocity classes tested, using the parallel code but only allowing use of a single CPU incurs a slowdown due to the overhead of passing objects into the parallelised functions.

In general the speedup decreases with the number of velocity classes, which indicates that there is significant overhead in parallelisation. With 2 CPUs we have speedup up to the case of 20 velocity classes. With 4 CPUs, the parallel algorithm results in significant speedup, above 60% in each case. The speedup for 5 velocity classes with 4 CPUs or more is obviously limited.

The Lindblad solver routine in the velocity class loop represents the most computationally-intensive part of the whole algorithm, so it is certainly useful to be able to make use of multiple core computers to perform these calculations. For the work described in this thesis we made use of an Intel Core i7 with up to 4 CPU cores, and for the most intensive calculations we used Durham University's *Hamilton* HPC Cluster with up to 12 CPU cores for each simulation.

Another process which could be computed in parallel is the iteration over timesteps $t_k$ (algorithm 1, line 7), which performs the weighted average over density matrix coherences to determine the polarisation of the medium at that time, and advances the field via the AB step. However, for the number of timesteps used in calculations we saw negligible speedup due to the high overhead required for this loop in passing arrays containing the polarisations and fields. In fact, for systems where less than $N_k = 1000$ timesteps are required for the necessary accuracy, this overhead caused the parallel implementation to be slower than the serial. It was therefore not used.

For fields with many modes, loops over these modes could be parallelised for computing polarisation. In this work we have only needed to consider systems of one or few modes, so it was not appropriate to implement parallelisation here.

# D  The Two-Step Adams-Bashforth Method with Varying Stepsize

Adams-Bashforth integration methods have a well-known derivation but we are not aware of a reference for the two-step method in the case that the two stepsizes are different, so we present the result here. This numerical method is used in solving the MB equations as described in chapterC. The two-step method requires two initial points, and the second point is calculated using a Euler step, which we wish to keep small to avoid introducing a large global error. The third point is then calculated with the Adams-Bashforth method with different step sizes. From then on the standard Adams-Bashforth method can be used.

We take an ordinary differential equation $y' = f(z, y(z))$ with an initial condition $y(z_0) = y_0$ that we wish to solve numerically. If we know $y(z)$ at a time $z_n$ and want to know what $z$ is at a later time $z_{n+1}$, the fundamental theorem of calculus tells us that we find it by integrating $y'$ over the time interval

$$y(z_{n+1}) = y(z_n) + \int_{z_n}^{z_{n+1}} y'(z) \, \mathrm{d}z = y(z_n) + \int_{z_n}^{z_{n+1}} f(z, y(z)) \, \mathrm{d}z. \quad \text{(D.1)}$$

The idea behind any ODE integrator is to compute the right-hand- side integral for some numerical approximation of $f$. The problem is then computed over a series of steps $n = 1, 2, \dots N$ to give a sequence of points $z_n$ which approximate $y(z)$ to some order of accuracy as a func-

tion of the stepsize. The method is consistent if the local error (*i.e.* the error from step $n$ to step $n + 1$) goes to zero faster than the stepsize $(z_{n+1} - z_n)$ goes to zero.

Where the Euler method takes the slope $f$ to be a constant on the interval $[z_n, z_{n+1}]$, the idea behind Adams-Bashforth methods is to approxmiate $f$ by a Lagrange interpolating polynomial[26]

$$P(z) = \sum_{j=1}^{m} P_j(z) \tag{D.2}$$

where

$$P_j(z) = y_j \prod_{\substack{k=1 \\ k \neq j}}^{m} \frac{z - z_k}{z_j - z_k}. \tag{D.3}$$

Here $P(z)$ is the polynomial of degree $\leq (m - 1)$ that passes through the $m$ points $(z_1, y_1 = f(z_1)), (z_2, y_2 = f(z_2)) \ldots (z_m, y_m = f(z_m))$. We'll take the linear $(m = 2)$ interpolant on the point $z_n$ and an earlier point $z_{n-1}$, so we have

$$P(z) = f(z_n, y_n) \frac{z - z_{n-1}}{z_n - z_{n-1}} + f(z_{n-1}, y_{n-1}) \frac{z - z_n}{z_{n-1} - z_n}. \tag{D.4}$$

Now if we substitute this approximating polynomial into the integral in (D.1), we find

$$\int_{z_n}^{z_{n+1}} f(z, y(z)) \, dz \approx \int_{z_n}^{z_{n+1}} P(z) \, dz$$

$$= \int_{z_n}^{z_{n+1}} \left[ f(z_n, y_n) \frac{z - z_{n-1}}{z_n - z_{n-1}} + f(z_{n-1}, y_{n-1}) \frac{z - z_n}{z_{n-1} - z_n} \right] dz$$

into which we may then put in the limits to obtain

$$\int_{z_n}^{z_{n+1}} f(z, y(z)) \, dz \approx \frac{(z_n - z_{n+1})}{2(z_{n-1} - z_n)} \Big[ f(z_n, y_n)(z_n + z_{n+1} - 2z_{n-1})$$

$$- f(z_{n-1}, y_{n-1})(z_n - z_{n+1}) \Big]. \tag{D.5}$$

If we let $h_1 := z_n - z_{n-1}$ and $h_2 := z_{n+1} - z_n$ then

$$\int_{z_n}^{z_{n+1}} P(z)\,\mathrm{d}z = \frac{h_2}{2h_1}\left[(2h_1 + h_2)f(z_n, y_n) - h_2 f(z_{n-1}, y_{n-1})\right].$$

Putting this back into the approximation of (D.1), we get

$$y(z_{n+1}) \approx y(z_n) + \frac{h_2}{2h_1}\left[(2h_1 + h_2)f(z_n, y_n) - h_2 f(z_{n-1}, y_{n-1})\right]$$

and our sequence of approximation points $y_n$ is calculated as

$$y_{n+1} = y_n + \frac{h_2}{2h_1}\left[(2h_1 + h_2)f(z_n, y_n) - h_2 f(z_{n-1}, y_{n-1})\right] \tag{D.6}$$

for $n = 1, 2, \ldots N$. This is the correct second-order Adams-Bashforth finite difference step in the case that the stepsizes are different.

If the steps are of equal size, i.e. $h := h_1 = h_2$ we find

$$y_{n+1} = y_n + \frac{3}{2}hf(z_n, y_n) - \frac{1}{2}hf(z_{n-1}, y_{n-1}) \tag{D.7}$$

which is the standard two-step Adams-Bashforth method.[27,28]

# Acknowledgements

I would like to thank...

# *Bibliography*

[1] J D Jackson. *Classical Electrodynamics*. Wiley, 1998.

[2] R W Boyd. *Nonlinear Optics*. Nonlinear Optics Series. Elsevier Science, 2008.

[3] E Hecht. *Optics*. Pearson Education, 2015.

[4] P Lambropoulos and D Petrosyan. *Fundamentals of Quantum Optics and Quantum Information*. Springer, 2007.

[5] D J Griffiths. *Introduction to Electrodynamics*. Prentice Hall, 1999.

[6] Mary B. James. Why the speed of light is reduced in a transparent medium, 1992.

[7] R P Feynman, R B Leighton, and M L Sands. *The Feynman Lectures on Physics*. Number v. 1 in The Feynman Lectures on Physics. Addison-Wesley, 1963.

[8] B H Bransden and C J Joachain. *Physics of Atoms and Molecules*. Pearson Education. Prentice Hall, 2003.

[9] G Grynberg, A Aspect, C Fabre, and C Cohen-Tannoudji. *Introduction to Quantum Optics: From the Semi-classical Approach to Quantized Light*. Cambridge University Press, 2010.

[10] C Cohen-Tannoudji, J Dupont-Roc, and G Grynberg. *Atom-photon interactions: basic processes and applications*. Wiley-Interscience publication. J. Wiley, 1992.

[11] Charles S. Adams and Erling Riis. Laser Cooling and Manipulation of Neutral Particles. pages 1–39, 1997.

[12] A. Icsevgi and W. E. Lamb. Propagation of light pulses in a laser amplifier. 1429, 1964.

[13] C J Foot. *Atomic physics*. Oxford master series in physics. Oxford University Press, 2005.

[14] J. Gea-Banacloche, Yong-qing Li, Shao-zheng Jin, and Min Xiao. Electromagnetically induced transparency in ladder-type inhomogeneously broadened media: Theory and experiment. *Physical Review A*, 51(1):576, 1995.

[15] R Loudon. *The Quantum Theory of Light*. OUP Oxford, 2000.

[16] L Allen and J H Eberly. *Optical Resonance and Two-level Atoms*. Dover books on physics and chemistry. Dover, 1975.

[17] a. V. Durrant. Some basic properties of stimulated and spontaneous emission: A semiclassical approach. *American Journal of Physics*, 44(7):630, 1976.

[18] Edwin Hewitt and Robert E. Hewitt. The Gibbs-Wilbraham phenomenon: An episode in fourier analysis. *Archive for History of Exact Sciences*, 21(2):129–160, 1979.

[19] Paul Siddons, Charles S. Adams, Chang Ge, and Ifan G. Hughes. Absolute absorption on rubidium D lines: comparison between theory and experiment. *Journal of Physics B: Atomic, Molecular and Optical Physics*, 41(15):155004, aug 2008.

[20] Daniel Adam Steck. Quantum and Atom Optics. page 932, 2007.

[21] W H Press. *Numerical Recipes 3rd Edition: The Art of Scientific Computing*. Cambridge University Press, 2007.

[22] C. De Boor. On calculating with B-splines. *Journal of Approximation Theory*, 6(1):50–62, 1972.

[23] Stéfan Van Der Walt, S. Chris Colbert, and Gaël Varoquaux. The NumPy array: A structure for efficient numerical computation. *Computing in Science and Engineering*, 13(2):22–30, 2011.

[24] Eric Jones, Travis Oliphant, Pearu Peterson, and Others. {SciPy}: Open source scientific tools for {Python}.

[25] P D Nation and J R Johansson. QuTiP : The Quantum Toolbox in Python. 2013.

[26] G B Arfken and H J Weber. *Mathematical Methods For Physicists International Student Edition*. Elsevier Science, 2005.

[27] L Edsberg. *Introduction to Computation and Modeling for Differential Equations*. Wiley, 2008.

[28] Francis Bashforth and John Couch Adams. *An attempt to test the theories of capillary action: by comparing the theoretical and measured forms of drops of fluid. With an explanation of the method of integration employed in constucting the tables which give the theoretical forms of such drops*. University Press, 1883.